ACS OMEGA

Open Access

http://pubs.acs.org/journal/acsodf

Article

Targeted Nanotherapy by Vinblastine-Loaded Chitosan-Coated PLA Nanoparticles to Improve the Chemotherapy via Reactive Oxygen Species to Hamper Hepatocellular Carcinoma

Amit Singh, Shivangi Bora, Pankaj Kumar, Ritushree Kukreti, and Mahima Kaushik*

Cite This: *ACS Omega* 2025, 10, 170−180

Read Online

ACCESS | Metrics & More | Article Recommendations | Supporting Information

ABSTRACT: Liver cancer is a prevalent and significant cause of death in humans. The use of novel biodegradable materials for various biomedical applications is being recently recommended as complementary as well as alternative solution for traditional chemotherapy. This study focuses on the synthesis of biodegradable nanocarriers [chitosan-coated poly(lactic acid) NPs (Cht-PLA NPs)] for the delivery of an anticancer drug vinblastine (Vbx) and to evaluate its therapeutic potential in human hepatocellular carcinoma (HepG2) cells. The Cht-PLA NPs were synthesized using the nanoprecipitation method and characterized by transmission electron microscopy, scanning electron microscopy, Fourier transform infrared spectroscopy, dynamic light scattering, and zeta potential techniques. The results showed that the nanoparticle sizes are in the range of 100−200 nm with positive surface charge. The release profile of the synthesized nanoformulation showed controlled release of the Vbx drug for 72 h. The anticancer efficacy of the synthesized nanoformulation was assessed on the HepG2 cell lines. The *in vitro* cytotoxicity study revealed that the Vbx-loaded Cht-PLA NPs showed higher toxicity with an increase in concentration as compared to the Vbx alone. Additionally, an *in vitro* cellular uptake study revealed higher internalization as compared to the drug alone due to the chitosan coating. Further, the ability to stimulate the reactive oxygen species (ROS) generation and variation in mitochondrial membrane potential at the IC_{50} concentration of Vbx-loaded Cht-PLA NPs was confirmed by using 2,7-dichlorodihydrofluorescein diacetate and rhodamine 123 dyes, respectively, and were analyzed under fluorescence microscopy. Hence, the results showed that Vbx-loaded Cht-PLA NPs possess high anticancer activity due to its higher cellular toxicity, cellular uptake, increased ROS production, and disruption in mitochondrial membrane potential. All these properties of the synthesized nanoformulation suggest it's potential applications in drug delivery systems, targeting liver cancer.

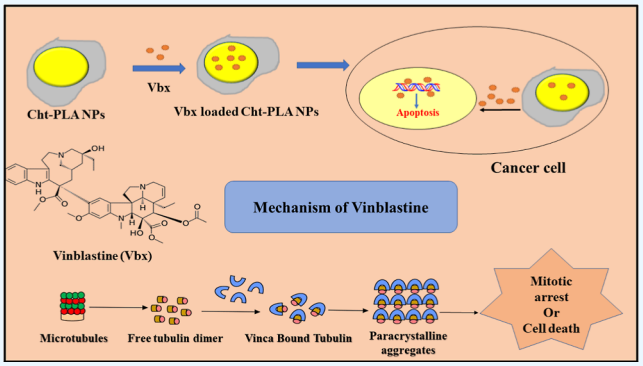

1. INTRODUCTION

Liver cancer stands as one of the most prevalent cancers globally, and unfortunately, a large number of liver cancer patients succumb to the disease within a year.[1] According to GLOBOCAN 2022 estimates, it is the sixth most commonly diagnosed cancer and the third leading cause of cancer-related deaths with 7.8% new cases from 20 million total cancer cases in 2022.[2] Liver cancer is also the second most common cause of premature cancer deaths.[2] Hepatocellular carcinoma (HCC) is a most common type of primary liver cancer, which contains prevalent malignant solid tumors with particularly poor prognosis and low survival rate among humans.[3,4] It has been reported that HCC-related deaths rank second highest among all cancer-related deaths worldwide.[5] The treatment options for this life-threatening disease encompass both surgical approaches such as liver resection and transplantation and non-surgical techniques like chemotherapy.[6] Liver cirrhosis, a condition often associated with HCC, stands as the primary underlying cause of HCC-related deaths in patients.[7]

Recently, there has been a significant surge in the utilization of nanoparticles (NPs) for medical purposes, particularly in the field of drug delivery. NPs made from various materials such as polymers, lipids, and inorganic compounds have been extensively studied, particularly in the context of cancer therapy.[8−12] These colloidal-sized particles typically range in size from 1 to 1000 nm and can either encapsulate drugs within their structure or attach them to their surface.[13−15] The limitation of traditional medicines is shifting the research toward nanotechnology-based alternatives.[16,17]

Received: April 7, 2024
Revised: September 13, 2024
Accepted: September 19, 2024
Published: December 20, 2024

Vinblastine (Vbx) is one of the first plant-derived chemotherapeutic agent that has been widely utilized in clinical settings for treating various cancers such as Hodgkin's disease, testicular cancer, ovarian cancer, breast cancer, head and neck cancer, and non-Hodgkin's lymphoma.[18,19] It exerts its effects by binding to tubulin, leading to the disruption of the microtubule assembly and interfering with the formation of the mitotic spindle. This ultimately results in mitotic arrest.[20,21] Vbx is regarded as an effective and exceptional drug, earning its place on the World Health Organization's List of Essential Medicines (WHO Model List of Essential Medicines; World Health Organization, 2021).[22] However, patients who receive Vbx treatment often experience systemic delivery and unpleasant side effects such as myelosuppression (leucopenia and anemia), inappropriate antidiuretic hormone secretion, ileus, mucositis, neuropathy, and Raynaud's phenomenon.[23−25]

Polymeric NPs have gained significant attention due to their inherent advantages in the controlled delivery of various therapeutic agents, such as human growth hormone, insulin, antitumor agents, proteins, and peptides. They offer localized or targeted drug delivery to specific tissue and organ sites with optimal release rates. One notable benefit of using the polyester family polymers, including poly(D,L-lactide-*co*-glycolide) (PLGA), polyglycolide (PGA), and polylactide (PLA), has garnered significant attention due to their excellent biocompatibility and biodegradability, along with their higher stability in biological fluids and during storage.[26−28] Furthermore, the hydrophobic nature of polyesters such as PLA and PLGA contributes to their slow degradation rate, which may limit their suitability for certain therapeutic applications.[29,30] Additionally, studies have indicated that when PLA and PLGA based NPs are delivered into the bloodstream, they can be rapidly cleared in the liver and captured by the reticuloendothelial system (RES).[31] However, these limitations can be addressed by incorporating chitosan into the hydrophobic PLA backbone, thereby overcoming the drawbacks associated with slow degradation and RES capture.

We have selected the PLA polymer in this study in place of other polymers due to its biocompatibility, biodegradability, and stretch ability. The polymer when degrades inside the acidic medium of the cancer cell, it breaks into lactic acid and its short oligomers, which are naturally recognized and metabolized by the body.[32,33] This inherent biocompatibility of PLA reduces the likelihood of triggering significant immune responses, but there is still a need to enhance its characteristics for drug delivery applications. One major drawback of PLA is its extremely high hydrophobicity, which makes it unsuitable for delivering hydrophilic drugs. To address these issues, various methods can be employed to improve its properties, such as surface modification. Blending PLA with hydrophilic polymers, like chitosan, can enhance its hydrophilicity.[34,35] Chitosan as a cationic surfactant was chosen as a drug carrier due to its favorable physicochemical properties and versatility.[14] The conventional chemotherapeutic drug faces challenges such as poor absorption and instability of the gastrointestinal tract (GI). Chitosan contains amino groups with a pK_a = 6.5, which become fully protonated at around pH 4, increasing the positive charge of chitosan. This positively charged chitosan interacts with mucin (negatively charged), leading to prolonged contact between the drug and the absorptive surface. Moreover, chitosan's mucoadhesive properties and its ability to transiently open tight junctions in the mucosal cell membrane enhance drug absorption in the stomach and duodenum compared to formulations without chitosan.[36,37] Furthermore, chitosan can inhibit certain transporter proteins on the membrane of intestinal epithelial cells, known as efflux pumps, which contribute to drug resistance.[38,39] Therefore, using a polymeric drug delivery system such as Cht-PLA NPs is an ideal strategy to improve drug bioavailability and intestinal absorption. Currently, the potential of polymeric nanocarriers for the intracellular delivery by coating with siRNA, aptamer, etc., in NP-based anticancer therapy is under investigation. Various studies involve the co-delivery of chemotherapeutic drugs and small siRNA using advanced polymeric NPs with pH-responsive and PEG-detachable features.[40] Utilizing a single type of NP for both cancer detection and drug delivery highlights their promise as theranostic tools for various diseases. These polymeric nanocarriers are being engineered with regions that respond to stimuli such as redox potential, temperature, pH, and light, making them effective for targeted cancer therapy.[41,42]

In this study, we have synthesized and characterized Cht-PLA NPs loaded with Vbx drug. The characterization of the nanoformulation involved the use of scanning electron microscopy (SEM), transmission electron microscopy (TEM), dynamic light scattering (DLS), zeta potential, and fourier transform infrared (FT-IR) spectroscopy. Furthermore, we have evaluated the potential of Cht-PLA NPs as carriers for Vbx through assessments of drug encapsulation and *in vitro* drug release. Also, *in vitro* studies are performed on HepG2 cell lines, such as cytotoxicity studies (MTT assay) and cellular uptake. Additionally, we expanded our investigation to examine the effect of Vbx-loaded Cht-PLA NPs on reactive oxygen species generation using DCFH-DA dye and disruption in mitochondrial membrane potential via rhodamine 123 assay. All these studies have resulted in identifying and fabricating a novel nanoformulation/nanotherapy, which may be explored further for its complementary as well as alternative use for lung cancer therapy.

2. MATERIALS AND METHODS

2.1. Materials. Poly(D,L lactide) 10 000−18 000, chitosan, vinblastine sulfate salt V1377, 3-(4,5-dimethylthiazol-2-yl)-2,5-diphenyltetrazolium bromide (MTT), rhodamine-123, 2-7-dichlorofluorescin diacetate (DCFH-DA), and a dialysis bag (12,000 Da) were procured from Sigma-Aldrich, Germany. The solvents such as acetic acid, acetone, methanol, acetonitrile, and triethylamine were of high-purity HPLC grade and purchased from Merck.

For *in vitro* experiments, HepG2 cell lines were procured from NCCS, Pune, India; Dulbecco's modified Eagle's medium (DMEM) with the GlutaMAX supplement; trypsin−EDTA solution (Gibco); antibiotic-antimycotic (100-X), and 10% fetal bovine serum were obtained from Gibco. All of the chemicals used in experiments were of pure commercial grade.

2.2. Synthesis of Chitosan-Coated PLA NPs. The synthesis of PLA and chitosan-coated PLA NPs followed a modified version of the well-established double-emulsion solvent evaporation method described by Dhanapal et al.[43] To initiate the process, the organic phase was prepared by dissolving 50 mg of PLA polymer in 5 mL of acetone (solvent A), while the aqueous phase was prepared by dispersing 5 mg of chitosan activated with 0.2% acetic acid in 45 mL of water (solvent B). Further, solvent A was carefully added drop by drop into solvent B, and the resulting mixture was sonicated for 5 min. Subsequently, the suspension was stirred overnight

https://doi.org/10.1021/acsomega.4c02983
ACS Omega 2025, 10, 170−180

on a magnetic stirrer. During this period, the polymer showed spontaneous self-assembly for the formation of NPs. To eliminate the excess unreacted chitosan, the NPs were subjected to dialysis (MW: 12,000 Da) against PBS (pH-7.4) for 3 h.

2.3. Characterization of NPs. *2.3.1. TEM and SEM Analysis.* The size and morphology of the NPs were determined by SEM and TEM analysis. TEM analysis was carried out on TALOS S CRYO-TEM (Thermo Scientific) with accelerating voltage at 200 kV. The samples were prepared by the drop-casting technique by taking 10 μL of sample on a carbon-coated grid and stained by phosphotungstic acid. The samples were dried at room temperature before analysis. The average size from the histogram was calculated by analyzing the image using image J software.

The SEM analysis was also carried out to examine the surface morphology of the NPs. The samples were analyzed by using a JEOL JSM-6610LV Scanning Electron Microscope. The samples for the SEM analysis were prepared using the same drop-casting technique onto a glass slide and dried overnight before analysis.

2.3.2. FT-IR Spectroscopy. FT-IR spectroscopy was used to understand the interaction, binding, and structure of the synthesized NPs and nanoformulations. The samples were prepared by the KBr pellet method, and the spectra were taken using a Thomas Scientific Spectrometer in the range of 400−4000 cm^{-1}.

2.3.3. DLS and Zeta Potential. The hydrodynamic size and polydispersity index (PDI) of the NPs were determined using Malvern Zetasizer Nano-ZS 90 dynamic light scattering. The samples for the analysis were prepared by diluting the sample 10 times, and the analysis was done in a disposable cuvette. The hydrodynamic size and PDI were reported by taking the mean of the three repeated measures.

Zeta potential was performed to understand the surface modification and the possibility of interaction between the ligands and the molecules. For the surface charge analysis, the zeta potential was performed on the same Malvern Zetasizer Nano-ZS-90. The electrophoretic mobility of the NPs was determined by using a laser Doppler electrophoretic method, which is then translated using automated software based on Henry's approximation. The samples were diluted 10 times for the analysis in a two-capped folded capillary.

2.3.4. Drug Encapsulation and In Vitro Release Study. To understand the drug encapsulation of the NPs, 10 mg of Vbx-loaded NPs was dissolved in 10 mL of DMSO solution and vortexed for 1 min. After that, methanol was added to precipitate the polymer. The mixture was vortexed and centrifuged, and the supernatant was removed by using a syringe filter of 0.45 μm pore size. The obtained sample was analyzed using HPLC (Thermo Fisher UltiMate 3000) equipped with a C-18 reversed-phase column (4.6 × 150 mm, 5 μm) and a UV−Visible detector at detection wavelength (269 nm) with 10 μL of injection volume. The mobile phase [acetonitrile/water (40:60, v/v) and 1.4% (v/v) triethylamine aqueous solution adjusted to pH 7.2 with phosphoric acid] were used throughout the experiment with 1.0 mL/min flow rate. The calibration curve was plotted from the obtained Vbx-loaded value. The entrapment efficiency was calculated by using the below equation

$$\%\ \mathrm{EE} = \frac{\text{actual drug loading}}{\text{theoretical drug loading}} \times 100$$

10 mg portion of the synthesized nanoformulation was dissolved in 50 mL of phosphate-buffered saline (pH = 7.4) and then transferred into the dialysis bag. After different time intervals (0, 1, 2, 3, 4, 6, 24, 48, and 72 h), 5 mL of release medium was taken out and replaced by the fresh PBS. The amount of Vbx released was analyzed by using HPLC. All the samples were analyzed in triplicate.

2.3.5. Stability Studies. The stability of Cht-PLA NPs and Vbx-loaded Cht PLA NPs were evaluated by observing changes in their size, PDI, and surface potential over nine months. The synthesized nanoformulations were stored at room temperature (25 °C) following the guidelines provided by the International Conference on Harmonization (ICH) Q1A (R2). The average size and surface charge of the NPs were determined at different time intervals (0, 3, 6, and 9 months) of storage. The samples were prepared by diluting in Milli-Q water and measured using a Malvern zetasizer at 25 °C.

2.3.6. Cell Culture. HepG2 cell lines were procured from the National Centre for Cell Science (NCCS) Pune, India. For the experiment, the cells were cultured in DMEM with 10% FBS, penicillin (100 U/ml), and streptomycin (100 μg/mL) incubated in a CO_2 incubator at 37 °C.

2.3.7. Cytotoxicity Assay. The MTT assay was performed to estimate the cell viability. This calorimetric assay depends on the NADPH cellular oxidoreductase enzyme, which helps in the estimation of viable cells. For the experiment, the cells were grown in a 96-well plate in a CO_2 incubator at 5% CO_2 and 37 °C conditions for 24 h. Following that, the medium was changed with new medium containing dosage. The cells were treated for 24 h in quadruplate (n = 4) with Vbx alone and Vbx-loaded Cht-PLA NPs at various doses (1.0−50 μg/mL). After treatment, the media was aspirated and washed with 1× PBS, and 0.5 mg/mL of MTT reagent was added to each well and incubated for 3 h in the CO_2 incubator. Later, the reagent was discarded, and 100 μL of DMSO was added; then, the reading was recorded at 570 nm with a reference filter of 630 nm using an Infinite 200 PRO multimode plate reader (Tecan, Mannedorf, Zurich, Switzerland).

2.3.8. Cell Uptake Study. The *in vitro* cellular uptake was performed using curcumin in place of Vbx due to its nonfluorescent nature. To monitor the cellular uptake, the study was conducted in two different groups of curcumin (cur) alone and cur-loaded Cht-PLA NPs. The HepG2 cell lines were cultured on the coverslips in a 6-well plate and subjected to treatments with curcumin alone and with Cht-PLA NPs loaded with curcumin at various time intervals (4, 6, and 24 h) at 37 °C with 5% CO_2. After treatment, the cells were rinsed with 1× PBS that was ice-cold for 5 min and mounted on the slides, and fluorescence imaging was performed by using a ZOE fluorescent cell imager from Bio-Rad.

2.3.9. Detection of ROS Damage. HepG2 cells were cultured in a 96-well plate and subjected to three separate treatments at IC_{50} concentration value of Vbx alone and Vbx-loaded Cht-PLA NPs for various time periods (4, 6, and 24 h). Following 40 min of incubation, the medium was changed by 10 mg/mL of 2,7-dichlorofluorescin diacetate (DCFH-DA). The intracellular reactive oxygen species (ROS) production was recorded at 485 nm (excitation) and 527 nm (emission) after 24 h using an Infinite 200 PRO multimode plate reader (Tecan, Mannedorf, Zurich, Switzerland).

2.3.10. Mitochondrial Damage. Rhodamine 123 dye (5 μg/mL) was employed to check the variation in the mitochondrial membrane potential by administering the Vbx-

https://doi.org/10.1021/acsomega.4c02983
ACS Omega 2025, 10, 170−180

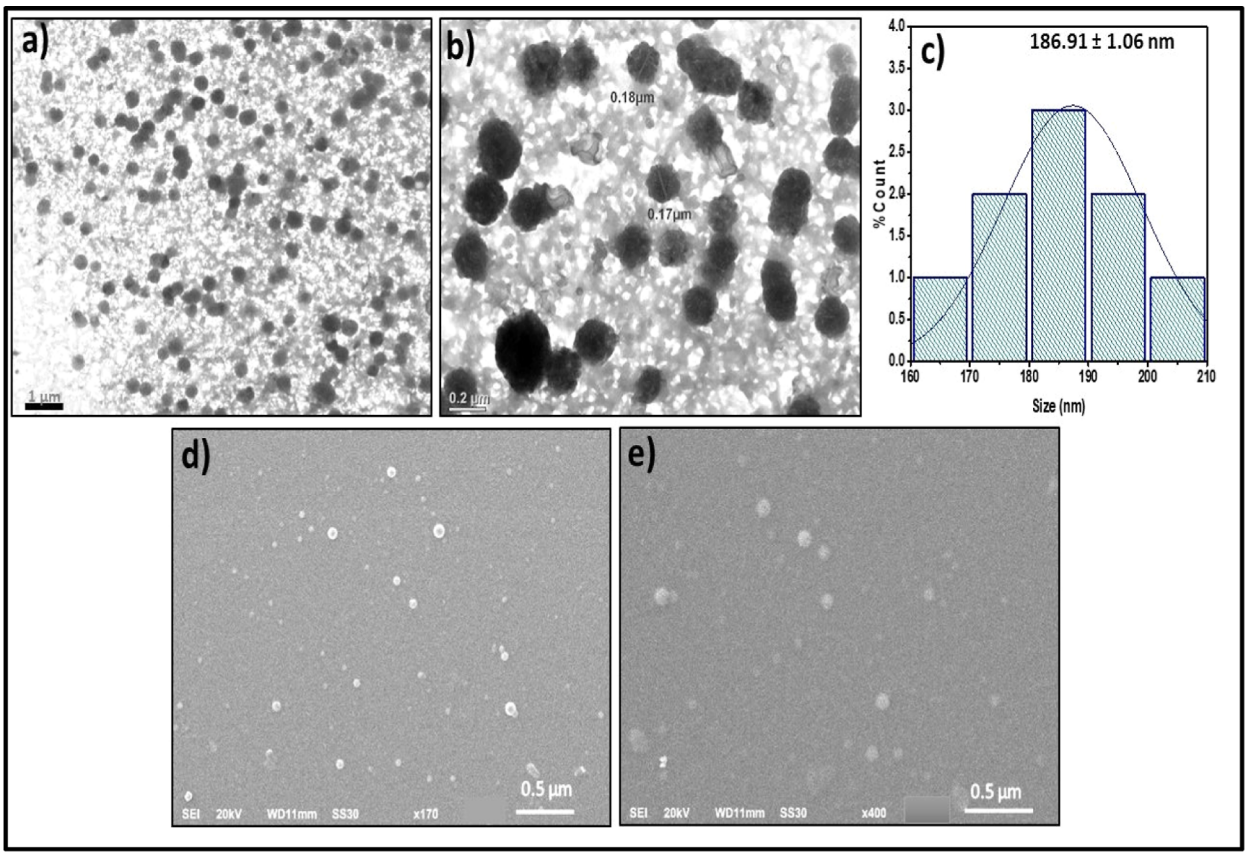

Figure 1. (a,b) TEM micrograph (magnification 1 and 0.2 μm); (c) size distribution histogram for Cht-PLA NPs; and (d,e) SEM images of the NPs (magnification 0.5 μm).

loaded Cht-PLA NPs to the HepG2 cancer cells. The inner membrane of the mitochondria is rich in negatively charged glycoprotein. The cationically charged rhodamine 123 preferably enters the mitochondria. The depolarization of the mitochondria membrane potential after treatment leads to the loss of rhodamine and a decrease in intensity. The released cytochrome-*c* from mitochondria to cytosol in the last stage of apoptosis after treatment with Vbx-loaded Cht-PLA NPs at the IC_{50} concentration was a glaring indication that the Vbx-loaded Cht-PLA NPs had an anticancer impact. Disruption in mitochondrial membrane potential was the first indication that Vbx-loaded Cht-PLA NPs and HepG2 cancer cells were undergoing apoptosis. In the experiment, the cells were seeded in a 6-well plate having coverslips and allowed to grow in serum and phenol red-free DMEM for 24 h in a CO_2 incubator.

After incubation, the cells were cleaned with 1× PBS, and rhodamine 123 dyes (5 μg/mL) were applied to the coverslip containing cells for 1 h. Once the stain had been incubated, it was removed by washing with 1× PBS. The treated and untreated cells were then compared under a fluorescent microscope to identify the HepG2 cell disrupted mitochondrial membrane potential.

3. RESULTS AND DISCUSSION

3.1. Characterization of NPs. Transmission and scanning electron microscopies are very useful techniques to understand the size, morphology, and formation of NPs. The TEM experiment was performed at two different magnifications, 1 μm (Figure 1a) and 0.2 μm (Figure 1b). The TEM images in Figure 1a,b showed that NPs were of uniform spherical shape without aggregation. The mean particle size was calculated by using a TEM histogram (Figure 1c), which showed that the particles were of approximately 186.91 ± 1.06 nm size, whereas the SEM images (Figure 1d,e) also showed that the particles were spherical in nature. The size of the NPs plays a crucial role in biodistribution and internalization in the target cell for potential delivery. The size of the NPs must not be too small (so that these can be easily excreted out) or not too large (so that these can be easily detected by the macrophages before reaching the target site).[14]

3.2. DLS, Zeta Potential, and Stability Study. The hydrodynamic sizes of the PLA and chitosan-coated PLA NPs were calculated by using the DLS technique, and the results are displayed in Figure 2a,b. The observed mean size of the Cht-PLA NPs was 220 ± 7.9 nm and that of PLA NPs was 190 ± 8.2 nm with a PDI value of 0.200 ± 0.001 and 0.250 ± 0.002, respectively. By modification of the surface of the NPs, an increase in size was observed, which was due to the coating of chitosan on the surface of NPs.

To confirm the coating of chitosan on the NPs, another experiment was conducted, where zeta potential was used to examine the change in the surface potential after surface modification. The zeta potential of the PLA alone (Figure 2c) was observed to be −24.91 ± 0.4 mV. The negative potential is due to the presence of a free carboxyl group of PLA on the surface of the NPs.[44] In the case of Cht-coated PLA NPs, the potential was 18.89 ± 0.9 mV (Figure 2d). The change or reversal in potential was due to the electrostatic deposition of the chitosan onto the surface of the NPs.[43]

https://doi.org/10.1021/acsomega.4c02983
ACS Omega 2025, 10, 170−180

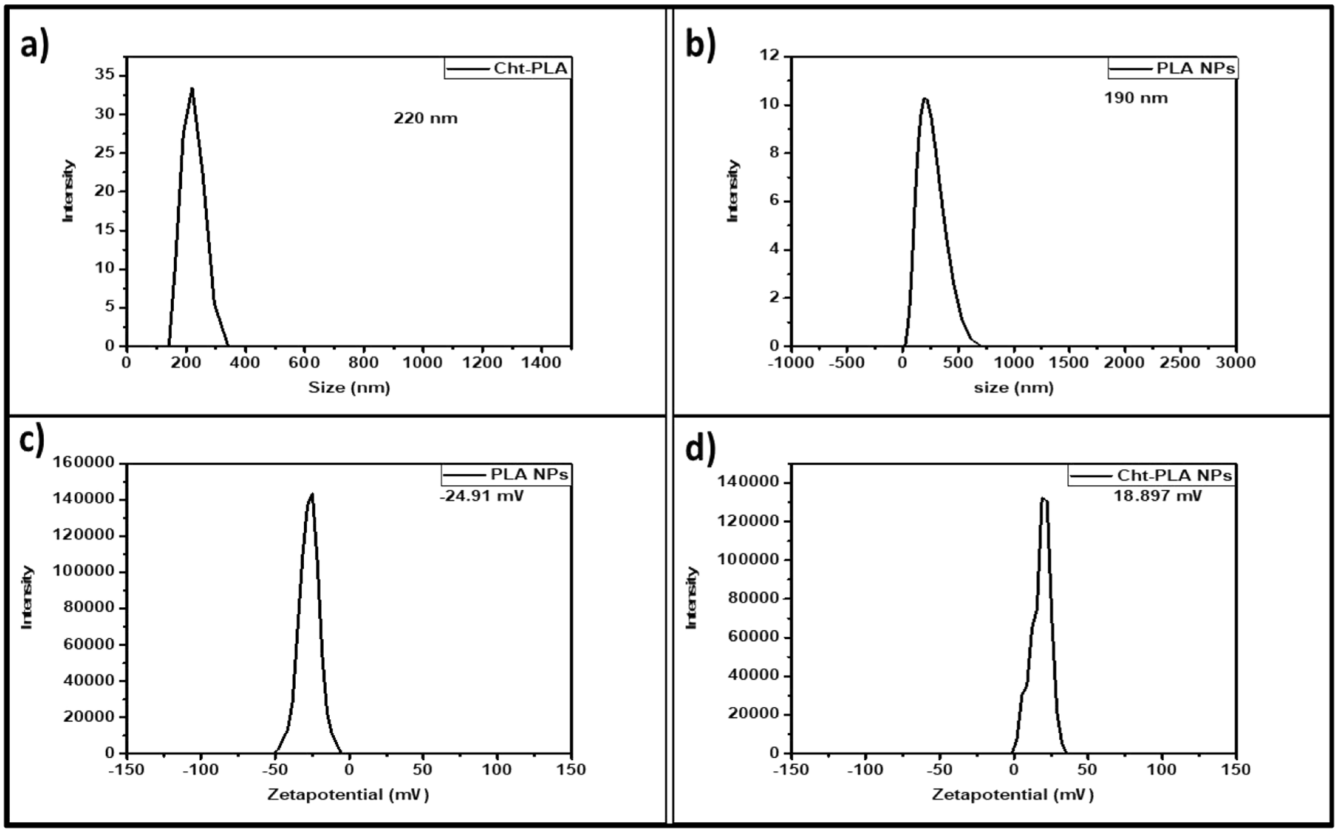

Figure 2. DLS spectrum of (a) Cht-PLA NPs and (b) PLA NPs (PDI, 0.200−0.250) and zeta potential spectrum of (c) PLA NPs and (d) Cht-PLA NPs.

Table 1. Particle Stability Studies after Different Time Intervals

time (months)	Cht-PLA NPs			Vbx-loaded Cht-PLA NPs		
	size (nm)	ZP (mV)	PDI	size (nm)	ZP (mV)	PDI
0	190 ± 8.2	18.72 ± 3.1	0.250 ± 0.002	220.28 ± 7.9	15.72 ± 2.1	0.200 ± 0.001
3	173.41 ± 4.9	19.18 ± 5.1	0.298 ± 0.001	230.41 ± 2.1	15.18 ± 5.7	0.268 ± 0.008
6	158.48 ± 3.8	13.88 ± 2.9	0.346 ± 0.003	170.21 ± 3.9	10.33 ± 1.9	0.410 ± 0.011
9	69.33 ± 5.2	9.33 ± 7.9	0.678 ± 0.016	130.34 ± 3.6	3.21 ± 6.3	0.613 ± 0.013

The stability studies of the nanoformulation Cht-PLA NPs and Vbx-loaded Cht-PLA NPs were performed as per ICH guidelines [http://www.ich.org/cache/compo/363-272-1.html#Q1A(R2)] for the assessment of their physical, chemical, and biological characteristics over time to detect any alterations that might develop.[45] Physical stability evaluation emphasizes key parameters like particle size, size distribution, PDI, and surface charge, all of which are susceptible to influences such as aggregation and precipitation etc. In our study, to analyze these parameters, techniques such as dynamic light scattering and zeta potential analysis are employed at 25 °C throughout fixed time intervals (0, 3, 6, and 9 months) as depicted in Table 1.[46] The average size and surface charge did not show a significant change in three months (Figure 3a,b), but after six months, the size and charge of the NPs start decreasing, and after 9 months, the NPs start losing their physical properties. The stability of Cht-PLA NPs for an extended period can be attributed to specific mechanisms. First, the positive charges present in chitosan interact with the negative charges on the NP surface, resulting in electrostatic stabilization. This electrostatic repulsion prevents particle aggregation, thereby maintaining the stability of the NPs

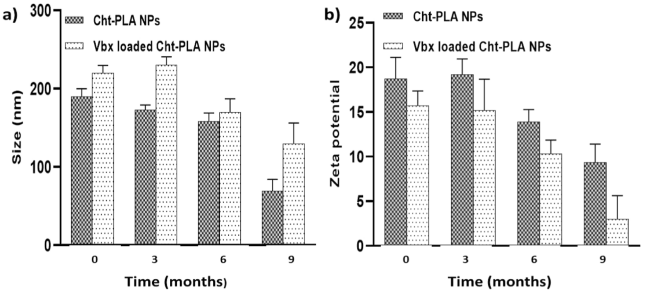

Figure 3. Stability of Cht-PLA NPs and Vbx-loaded Cht-PLA NPs: (a) average size of NPs and (b) zeta potential of suspension after synthesis immediately and 3, 6, as well as 9 months after storage at room temperature (25 °C).

dispersion. Moreover, the chitosan coating acts as a physical barrier, guarding the PLA NPs against external factors such as pH changes, enzymes, and environmental stresses. These effects play a crucial role in the stability of the NPs over time.[47,48]

3.3. FT-IR Spectroscopy. The FT-IR experiments were performed to understand the presence of different functional

https://doi.org/10.1021/acsomega.4c02983
ACS Omega 2025, 10, 170−180

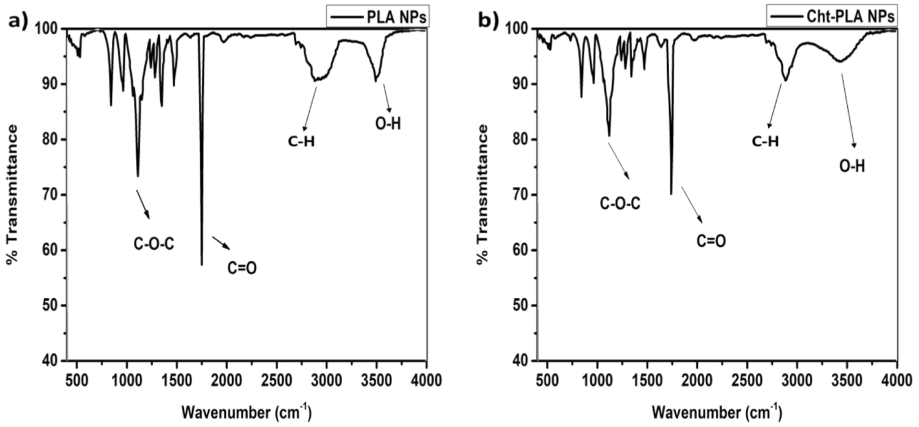

Figure 4. FT-IR spectrum of NPs: (a) PLA NPs and (b) Cht-PLA NPs.

groups and the type of interaction. The FT-IR spectrum of PLA in Figure 4a showed a characteristic carbonyl peak around 1700 cm^{-1}, and a stretching peak around 1100 cm^{-1} corresponds to the C−O−C functional group. The stretching vibration of the hydroxyl group (O−H) is broader in nature and is towards the lower wavenumber, due to their involvement in hydrogen bonding. The bands around 2900 cm^{-1} denoted the stretching of C−H of the CH_3 group.

To understand the binding of the chitosan to PLA, there are two major noticeable changes in the Cht-PLA NPs (Figure 4b). The peak around 1800 cm^{-1} belongs to the ester group of PLA and becomes weaker in intensity, while the hydroxyl and amino group around 3400 cm^{-1} pronouncedly decrease in intensity. All these confirm the interaction of the carboxyl, amino, and hydroxyl groups of chitosan with PLA. Other than that, the peak around 1700 cm^{-1} confirms the presence of carboxylate anions and $-NH_3^+$ of Cht-PLA NPs. This indicates that the grafting of chitosan has successfully occurred on the surface of PLA NPs.[37,43,49]

3.4. Drug Encapsulation and *In Vitro* Release Study. The entrapment efficiency of the polymeric NPs is majorly dependent on the composition of the copolymer, molecular weight, crystallinity, and hydrophobic and hydrophilic percentage.[50] From the experiment, the Vbx-loaded polymer showed 53 ± 6.83% of encapsulation efficiency.

For the release study, the drug is encapsulated in the PLA NPs and Cht PLA NPs, and the drug is released by diffusion or erosion in the PBS medium of pH 7.4. The parameters such as molecular weight, surface modification, particle size, hydrophobicity, and hydrophilicity ratio played a crucial role in drug release rate. In Figure 5, the PLA NPs showed that the drug release from NPs features an initial burst release from 0 to 6 h, followed by a slower, sustained release from 24 to 96 h. This pattern arises from the diffusion of the drug out of the polymer matrix and the gradual degradation of the polymer.[51] In the case of Vbx-loaded Cht-PLA NPs, the release study revealed that the Vbx-loaded Cht-PLA NPs showed slow release in the early stage due to the chitosan layer, which restricts the diffusion of the drug.[52] Over the next 24 h, the rate of release (52.43 ± 7.12%) increases until it becomes consistent. The PLA polymer is strongly hydrophobic in nature and has high drug permeability, whereas chitosan is a hydrophilic polymer.[53] The use of chitosan with PLA allowed water to infiltrate the copolymer's core and increase the drug release.[54,55] Thus, the Vbx-loaded Cht-PLA NPs exhibited a prolonged drug release

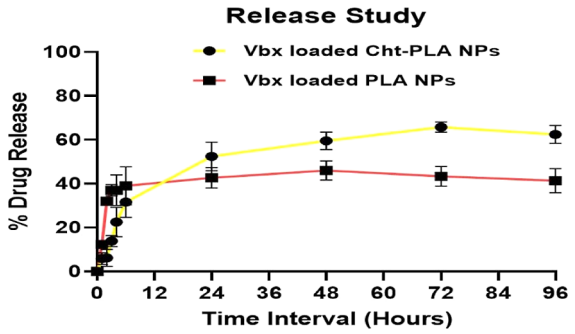

Figure 5. *In vitro* release profile of Vbx-loaded PLA NPs and Vbx-loaded Cht-PLA NPs in PBS (pH 7.4).

profile, indicating their potential as a sustained drug delivery system.[35]

3.5. *In Vitro* Cytotoxicity. The MTT 3-(4,5-dimethyl thiazol-2-yl)-2,5-diphenyl tetrazolium bromide assay is a quantitative method for assessing cell viability in response to the drug and drug-loaded NPs. The HepG2 cell line was used to examine the influence of Vbx alone and Vbx-loaded Cht-PLA NPs on *in vitro* cell viability. To assess the cytotoxicity, the cells were treated with various concentrations of drug-loaded NPs ranging from 1.0 to 50 μg/mL for 24 h. The results in Figure 6 showed a dose-dependent cytotoxic effect with both free and Vbx-loaded Cht-PLA NPs. The Vbx alone showed high toxicity at low concentration as compared to drug-loaded formulation due to suppressing the microtubule, which leads to inhibition of cell division. Whereas at higher concentration, Vbx causes microtubule depolymerization and leads to tubulin-vinblastine aggregates. This aggregation reduces the amount of free Vbx drug and results in a decrease in cytotoxicity.[56] However, Vbx-loaded Cht-PLA NPs (IC_{50} = 8.0 μg/mL) showed higher toxicity as compared to the Vbx alone (IC_{50} = 24 μg/mL) due to their cationically charged surface, which allows their easy interaction with cell membranes and lead to improved cellular internalization.[57] It has been suggested that the Cht-PLA NPs after degradation form monomers of lactic acid, which does not play any significant role in cytotoxicity, whereas the positive charge plays as a significant factor in the particle interaction and adherence to biological cells.[58] In general, it is believed that smaller particles less than around 100−200 nm can be internalized through receptor-mediated endocytosis, while bigger particles must be phagocytosed to be taken up.[59]

https://doi.org/10.1021/acsomega.4c02983
ACS Omega 2025, 10, 170−180

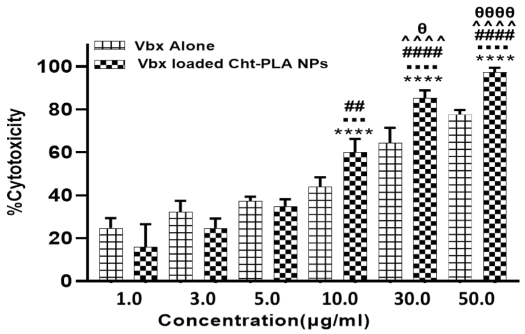

Figure 6. Dose-dependent cytotoxicity of Vbx alone and Vbx-loaded Cht-PLA NPs against HepG2 cells after 24 h of incubation. $^{****}p < 0.0001$ Vbx alone (1 μg/mL) vs Vbx-loaded Cht-PLA NPs (10, 30, and 50 μg/mL); $^{•••}p < 0.001$ Vbx alone (3 μg/mL) vs Vbx-loaded Cht-PLA NPs (10 μg/mL); $^{••••}p < 0.0001$ Vbx alone (3 μg/mL) vs Vbx-loaded Cht-PLA NPs (30, 50 μg/mL); $^{\#\#}p < 0.01$ Vbx alone (5 μg/mL) vs Vbx-loaded Cht-PLA NPs (30 μg/mL); $^{\#\#\#\#}p < 0.0001$ Vbx alone (5 μg/mL) vs Vbx-loaded Cht-PLA NPs (30, 50 μg/mL); $^{\hat{}\hat{}\hat{}\hat{}}p < 0.0001$ Vbx alone (10 μg/mL) vs Vbx-loaded Cht-PLA NPs (30, 50 μg/mL); $^{\theta}p < 0.1$ Vbx alone (30 μg/mL) vs Vbx-loaded Cht-PLA NPs (30 μg/mL): $^{\theta\theta\theta\theta}p < 0.0001$ Vbx alone (30 μg/mL) vs Vbx-loaded Cht-PLA NPs (50 μg/mL): $^{+}p < 0.5$ group II (4 h) vs group II (24 h); $^{•••}p < 0.001$ group I (6 h) vs group II (6 h); $^{\#\#\#\#}p < 0.0001$ group I (24 h) vs group II (24 h).

Thus, it is evident that Vbx-loaded Cht-PLA NPs exhibited more effective anticancer effect by inhibiting tumor growth in the case of HepG2 cell lines.

3.6. Cellular Uptake. The better and effective internalization and retention of the drug-loaded Cht-PLA NPs by the HepG2 cells, play a vital role in it therapeutic actions. To investigate the cellular uptake of NPs in *in vitro* studies, the most common experimental approach involves using fluorescent labeling such as curcumin, coumarin-6, etc. In this study, the vinblastine drug shows poor fluorescent property and cannot be used for the tracking of NPs; hence, for easy detection of the NPs inside the cell, curcumin was used as a florescent tag in fluorescence microscopy.[15] Then, quantitative analysis of the intensity of the treated cells were done by ImageJ software to assess the degree of particle absorption. In this experiment, the quantitative absorption of the Cht-PLA NPs with IC_{50} concentration at different time intervals (4, 6, and 24 h) was performed. Figure 7a displays fluorescence microscopic images of monolayers of HepG2 cells and after treatment for 4 h curcumin-loaded Cht-PLA NPs showed an increase in intensity with time up to 6 h and then decrease in intensity at 24 h. The results showed that Cht-PLA NPs exhibited greater cellular absorption with time, which may be attributed to their high cellular uptake and results in an increase in fluorescence intensity due to the cationic charge by the chitosan copolymer.[14] In contrast, curcumin exhibits a remarkable ability to selectively target cancer cells, which is

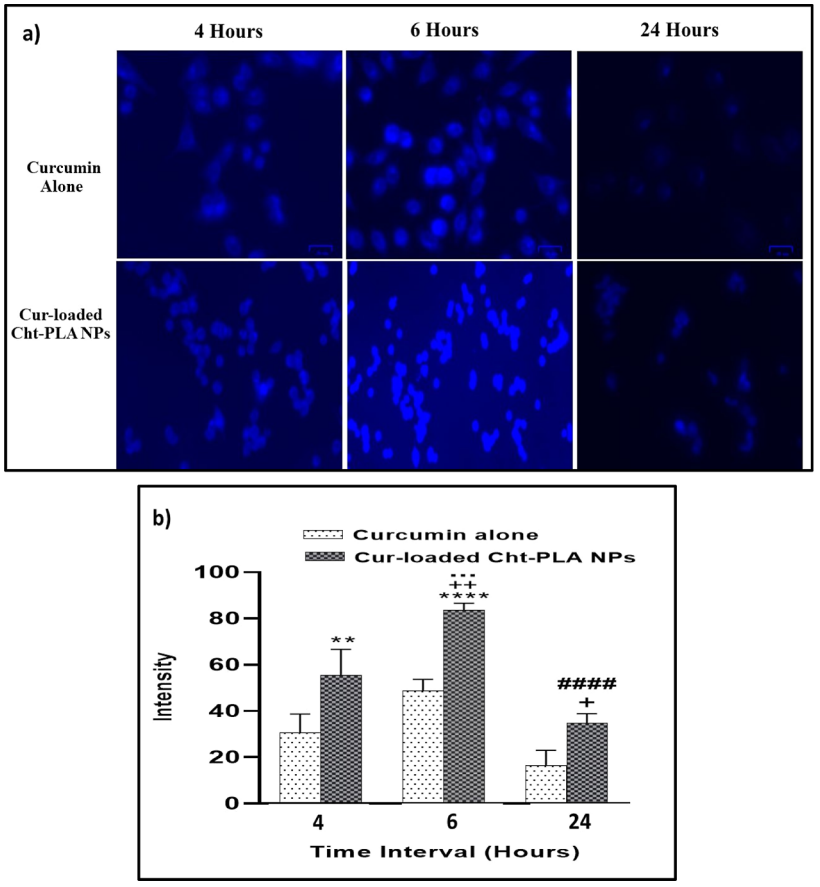

Figure 7. (a) Fluorescence microscopic images of HepG2 cells incubated with curcumin alone and Cur-loaded Cht-PLA NPs at 37 °C for 4, 6, and 24 h. (b) Quantitative analysis of uptake kinetics of curcumin alone (group I) and Cur-loaded Cht-PLA NPs. $^{**}p < 0.01$ group I (4 h) vs group II (4 h); $^{****}p < 0.0001$ group I (4 h) vs group II (6 h); $^{++}p < 0.01$ group II (4 h) vs group II (6 h); $^{+}p < 0.5$ group II (4 h) vs group II (24 h); $^{•••}p < 0.001$ group I (6 h) vs group II (6 h); $^{\#\#\#\#}p < 0.0001$ group I (24 h) vs group II (24 h).

https://doi.org/10.1021/acsomega.4c02983
ACS Omega 2025, 10, 170−180

potentially attributed to its interactions with multiple signaling pathways that play a crucial role in the survival and proliferation of cancer cells.[60] Our findings demonstrated that the synthesized Cht-PLA NPs had greater cellular absorption as compared to curcumin alone, which can be easily shown from the quantitative analysis (Figure 7b). The increase in fluorescence intensity with time governs the increase in uptake, whereas at 24 h, the fluorescence decreases due to cells leading to the apoptosis. This explains the significant benefits of the nanoformulation for the development of drug carriers in drug delivery systems.

3.7. *In Vitro* ROS Analysis. The ROS generation analysis is an important study that focuses on the ROS formation in cancer cells caused by oxidative stress reactions that are induced by treatment.[60] The DCFH-DA fluorescent dye is a promising candidate for the estimation of ROS generation. The IC_{50} concentration was used for the treatment of HepG2 cancer cells at different time intervals (4, 6, and 24 h). The results showed the increase in ROS from 4 to 6 h and then decline at 24 h in both the cases, as shown in Figure 8. The

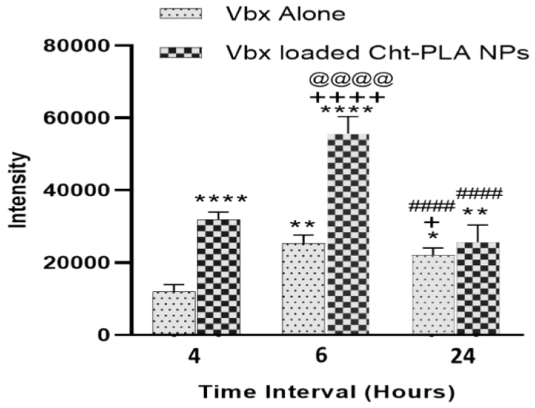

Figure 8. Quantification of ROS production of Vbx alone (group I) and Vbx-loaded Cht-PLA NPs (group II) against HepG2 using DCFH-DA fluorescent dye.****$p < 0.0001$ group I (4 h) vs group II (4 h), (6 h); **$p < 0.01$ group I (4 h) vs group I (6 h), group II (24 h); *$p < 0.5$ group I (4 h) vs group I (24 h); $^{++++}p < 0.0001$ group II (4 h) vs group II (6 h); $^{+}p < 0.5$ group II (4 h) vs group I (24 h); $^{@@@@}p < 0.0001$ group I (6 h) vs group II (6 h); $^{\#\#\#\#}p < 0.0001$ group II (6 h) vs group I (24 h), group II (24 h).

Vbx-loaded Cht-PLA NPs showed high ROS generation, due to its high cellular uptake, which results in higher internalization of the drug, whereas the Vbx alone has poor solubility and results in lesser cellular uptake and low ROS generation. The Vbx-loaded Cht-PLA NPs have anticancer capabilities, as a result of the ROS activation. The polymeric nanoformulation itself does not contribute to the ROS generation, unless there is any specific modification on it.[61−63] The drug-loaded NPs generate ROS in HepG2 cancer cells after the appropriate amount of time, and this generated ROS gets accumulated on the DNA granules, which destroys the DNA's capacity to transfer and prevented the formation of the polymerase enzyme.[64] After treatment, the DNA's ability was compromised, and the immature DNA was condensed and flowed out, which was later bound by DCFH-DA dye and displayed structural deformity.[65] Additionally, the oxidative stress response decreased the activity of genes involved in apoptosis and caused programmed cell death, as a result of intracellular leakages in the mitochondrial membrane.[66,67] Therefore, the current findings demonstrated that Vbx-loaded Cht-PLA NPs have a greater capacity to prevent the development of cancer cells via oxidative-stress-mediated ROS production.

3.8. Mitochondrial Damage. Rhodamine 123 is a dye, which is used for spotting a cancer cell-altered membrane architecture. It disrupts the intrinsic mechanism involved in the cell cycle process in cancer. It can adhere to injured cells and bind to negatively charged inner mitochondrial membranes.[65] Monitoring the depolarized mitochondrial membrane, which is caused by the failure of the responsive genes, is crucial. Caspases are triggered, when the mitochondrial membrane is disrupted, which lowers the production of genes that are receptive to cancer cells and activates the BCL-2 suppressive genes.[64,68] Our findings made the inhibition of HepG2 cells at IC_{50} concentrations of Vbx-loaded Cht-PLA NPs. It can be said that the number of necrotic and apoptotic cells was higher in treated cells compared to control cells (Figure S1a,b). Due to the increased activation of responsive genes, it caused repeated life cycle arrests in cancer cells and initiated the cascade of the apoptotic cell receptor. It is the first step in starting apoptosis. The outcome of Figure S1ab revealed that apoptotic cells were seen to be rough, loosely connected and had a highly necrotic character. In contrast, Figure S1a depicts the morphological colonies that were found to be smooth, compact, and clumped. Our findings referred to the decrease of red color intensity which was quantified by using ImageJ software and showed in Figure S1c as a noteworthy drop in binding of rhodamine 123 dye due to depolarization of mitochondrial membrane potential.[69,70]

4. CONCLUSIONS

The Vbx-loaded Cht-PLA NPs were synthesized and characterized by various techniques, including SEM, TEM, DLS, FT-IR, and zeta potential. Moreover, the results from the *in vitro* cytotoxicity and cellular uptake study demonstrated that the incorporation of the drug into the nanoformulation significantly enhanced its cytotoxicity and cellular uptake, compared to the administration of the drug alone. Vbx-loaded Cht-PLA NPs exhibited remarkable anticancer activity against HepG2 cells, inducing extensive damage to the mitochondrial membrane. Moreover, the generation of ROS was substantially elevated, as confirmed by fluorescent microscopic analysis using the DCFH-DA dye and rhodamine 123. The research findings of this work indicate that the Vbx-loaded Cht-PLA NP system holds great potential as a vehicle for delivering chemotherapeutic agents and enhancing cytotoxicity in HepG2 cells. These encouraging results strongly support the anticancer efficacy of the designed nanoformulation; however, more *in vivo* studies may be needed further for supporting this hypothesis.

■ ASSOCIATED CONTENT

Supporting Information

The Supporting Information is available free of charge at https://pubs.acs.org/doi/10.1021/acsomega.4c02983.

Mitochondrial damage analysis by using rhodamine 123 dye to understand the effect of the Vbx-loaded Cht-PLA NPs on the HepG2 cell line (PDF)

https://doi.org/10.1021/acsomega.4c02983
ACS Omega 2025, 10, 170−180

AUTHOR INFORMATION

Corresponding Author

Mahima Kaushik − *Nano-bioconjugate Chemistry Lab, Cluster Innovation Centre, University of Delhi, Delhi 110007, India;* orcid.org/0000-0002-6453-076X; Phone: +91-11-27666706; Email: mkaushik@cic.du.ac.in

Authors

Amit Singh − *Nano-bioconjugate Chemistry Lab, Cluster Innovation Centre, University of Delhi, Delhi 110007, India; Department of Chemistry, University of Delhi, Delhi 110007, India*

Shivangi Bora − *Genomics and Molecular Medicine Unit, Institute of Genomics and Integrative Biology (IGIB)-Council of Scientific and Industrial Research (CSIR), Delhi 110007, India*

Pankaj Kumar − *Nano-bioconjugate Chemistry Lab, Cluster Innovation Centre, University of Delhi, Delhi 110007, India; Department of Chemistry, University of Delhi, Delhi 110007, India*

Ritushree Kukreti − *Genomics and Molecular Medicine Unit, Institute of Genomics and Integrative Biology (IGIB)-Council of Scientific and Industrial Research (CSIR), Delhi 110007, India; Academy of Scientific and Innovative Research (AcSIR), Ghaziabad 201002 Uttar Pradesh, India*

Complete contact information is available at: https://pubs.acs.org/10.1021/acsomega.4c02983

Notes

The authors declare no competing financial interest.

ACKNOWLEDGMENTS

Authors appreciate the constant support and encouragement from Prof. Shrikant Kukreti [Department of Chemistry, University of Delhi, Delhi]. We would also like to acknowledge Prof. Pradeep Kumar [Senior Principal Scientist, I.G.I.B., Mall Road, Delhi] for extending his lab facilities. Also, Faculty Research Programme (FRP) grant by Institute of eminence (IoE) from University of Delhi, Delhi [ref. no./IoE/2021/12/FRP], is sincerely acknowledged. A.S., and P.K. are thankful for their fellowships [ref. no. Sch/139/Non-Net/Chem./Ph.D/2018-19/625] to Dept. of Chemistry, Delhi University, and CSIR, Delhi [CSIR fellowship no. 09/045(1646)/2019-EMR-1], respectively.

REFERENCES

(1) Wu, B.; Liang, Y.; Tan, Y.; Xie, C.; Shen, J.; Zhang, M.; Liu, X.; Yang, L.; Zhang, F.; Liu, L.; et al. Genistein-loaded nanoparticles of star-shaped di-block copolymer mannitol-core PLGA-TPGS for the treatment of liver cancer. *Mater. Sci. Eng., C* **2016**, *59*, 792−800.

(2) Bray, F.; Laversanne, M.; Sung, H.; Ferlay, J.; Siegel, R. L.; Soerjomataram, I.; Jemal, A. Global cancer statistics 2022: GLOBOCAN estimates of incidence and mortality worldwide for 36 cancers in 185 countries. *Ca-Cancer J. Clin.* **2024**, *74* (3), 229−263.

(3) Weledji, E. P.; Orock, G. E.; Ngowe, M. N.; Nsagha, D. S. How grim is hepatocellular carcinoma? *Ann. Med. Surg.* **2014**, *3* (3), 71−76.

(4) Bhattacharya, S.; Mondal, L.; Mukherjee, B.; Dutta, L.; Ehsan, I.; Debnath, M. C.; Gaonkar, R. H.; Pal, M. M.; Majumdar, S. Apigenin loaded nanoparticle delayed development of hepatocellular carcinoma in rats. *Nanomed. Nanotechnol. Biol. Med.* **2018**, *14* (6), 1905−1917.

(5) Jarnagin, W.; Chapman, W. C.; Curley, S.; D'Angelica, M.; Rosen, C.; Dixon, E.; Nagorney, D. Surgical treatment of hepatocellular carcinoma: expert consensus statement. *HPB* **2010**, *12* (5), 302−310.

(6) Smith, R. J. Nutrition and metabolism in hepatocellular carcinoma. *Hepatobiliary Surg. Nutr.* **2013**, *2* (2), 89.

(7) Sears, J. E.; Boger, D. L. Total synthesis of vinblastine, related natural products, and key analogues and development of inspired methodology suitable for the systematic study of their structure−function properties. *Accounts Chem. Res.* **2015**, *48* (3), 653−662.

(8) De Jong, W. H.; Borm, P. J. Drug delivery and nanoparticles: applications and hazards. *Int. J. Nanomed.* **2008**, *3* (2), 133−149.

(9) Gref, R.; Minamitake, Y.; Peracchia, M. T.; Trubetskoy, V.; Torchilin, V.; Langer, R. Biodegradable long-circulating polymeric nanospheres. *Science* **1994**, *263* (5153), 1600−1603.

(10) Labhasetwar, V.; Song, C.; Levy, R. J. Nanoparticle drug delivery system for restenosis. *Adv. Drug Delivery Rev.* **1997**, *24* (1), 63−85.

(11) Sinha, V. R.; Bansal, K.; Kaushik, R.; Kumria, R.; Trehan, A. Poly-ε-caprolactone microspheres and nanospheres: an overview. *Int. J. Pharm.* **2004**, *278* (1), 1−23.

(12) Chaudhary, S.; Singh, A.; Kumar, P.; Kaushik, M. Strategic targeting of non-small-cell lung cancer utilizing genetic material-based delivery platforms of nanotechnology. *J. Biochem. Mol. Toxicol.* **2021**, *35* (7), No. e22784.

(13) Sonia; Singh, A.; Kukreti, R.; Kukreti, R.; Kukreti, S.; Kaushik, M. Probing multifunctional azure B conjugated gold nanoparticles with serum protein binding properties for trimodal photothermal, photodynamic, and chemo therapy: Biophysical and photophysical investigations. *Biomater. Adv.* **2022**, *134*, 112678.

(14) Singh, A.; Bora, S.; Khurana, S.; Kumar, P.; Sarkar, N.; Kukreti, R.; Kukreti, S.; Kaushik, M. Advance nanotherapeutic approach for systemic co-delivery of mitoxantrone loaded chitosan coated PLGA nanoparticles to improve the chemotherapy against human non-small cell lung cancer. *J. Drug Delivery Sci. Technol.* **2023**, *84*, 104523.

(15) Prabu, P.; Chaudhari, A. A.; Dharmaraj, N.; Khil, M. S.; Park, S. Y.; Kim, H. Y. Preparation, characterization, in-vitro drug release and cellular uptake of poly (caprolactone) grafted dextran copolymeric nanoparticles loaded with anticancer drug. *J. Biomed. Mater. Res., Part A* **2009**, *90* (4), 1128−1136.

(16) Mei, L.; Zhang, Z.; Zhao, L.; Huang, L.; Yang, X. L.; Tang, J.; Feng, S. S. Pharmaceutical nanotechnology for oral delivery of anticancer drugs. *Adv. Drug Delivery Rev.* **2013**, *65* (6), 880−890.

(17) Yan, F.; Zhang, C.; Zheng, Y.; Mei, L.; Tang, L.; Song, C.; Sun, H.; Huang, L. The effect of poloxamer 188 on nanoparticle morphology, size, cancer cell uptake, and cytotoxicity. *Nanomed. Nanotechnol. Biol. Med.* **2010**, *6* (1), 170−178.

(18) Sears, J. E.; Boger, D. L. Total synthesis of vinblastine, related natural products, and key analogues and development of inspired methodology suitable for the systematic study of their structure−function properties. *Accounts Chem. Res.* **2015**, *48* (3), 653−662.

(19) Zhu, Y.; Liu, R.; Huang, H.; Zhu, Q. Vinblastine-loaded nanoparticles with enhanced tumor-targeting efficiency and decreasing toxicity: developed by one-step molecular imprinting process. *Mol. Pharmaceutics* **2019**, *16* (6), 2675−2689.

(20) Guerrieri, P.; Montemaggi, P.; Rubin, R.; Limbergen, E.; Troicki, F. T.; Poli, J.; Rubin, R.; Troicki, F. T.; Poli, J.; Brashears, J. H.; et al. Vinca alkaloids. In *Encyclopedia of Radiation Oncology*, 2013; p 949..

(21) O'Marcaigh, A. S.; Betcher, D. L. The vinca alkaloids. *J. Pediatr. Oncol. Nurs.* **1995**, *12* (3), 140−142.

(22) *WHO Model List of Essential Medicines*; World Health Organization, 2021.

(23) Jin, S.; Wan, J.; Meng, L.; Huang, X.; Guo, J.; Liu, L.; Wang, C. Biodegradation and toxicity of protease/redox/pH stimuli-responsive PEGlated PMAA nanohydrogels for targeting drug delivery. *ACS Appl. Mater. Interfaces* **2015**, *7* (35), 19843−19852.

(24) Marinina, J.; Shenderova, A.; Mallery, S. R.; Schwendeman, S. P. Stabilization of vinca alkaloids encapsulated in poly (lactide-co-glycolide) microspheres. *Pharm. Res.* **2000**, *17*, 677−683.

(25) Chong, C. D.; Logothetis, C. J.; Savaraj, N.; Fritsche, H. A.; Gietner, A. M.; Samuels, M. L. The correlation of vinblastine pharmacokinetics to toxicity in testicular cancer patients. *Br. J. Clin. Pharmacol.* **1988**, *28* (8), 714−718.
(26) Feng, S. S.; Chien, S. Chemotherapeutic engineering: application and further development of chemical engineering principles for chemotherapy of cancer and other diseases. *Chem. Eng. Sci.* **2003**, *58* (18), 4087−4114.
(27) Ahlin, P.; Kristl, J.; Kristl, A.; Vrečer, F. Investigation of polymeric nanoparticles as carriers of enalaprilat for oral administration. *Int. J. Pharm.* **2002**, *239* (1−2), 113−120.
(28) Cavalli, R.; Bargoni, A.; Podio, V.; Muntoni, E.; Zara, G. P.; Gasco, M. R. Duodenal administration of solid lipid nanoparticles loaded with different percentages of tobramycin. *J. Pharmaceut. Sci.* **2003**, *92* (5), 1085−1094.
(29) Park, W.; Kim, D.; Kang, H. C.; Bae, Y. H.; Na, K. Multi-arm histidine copolymer for controlled release of insulin from poly (lactide-co-glycolide) microsphere. *Biomaterials* **2012**, *33* (34), 8848−8857.
(30) Wang, Z.; Wu, Y.; Zeng, X.; Ma, Y.; Liu, J.; Tang, X.; Gao, Y.; Liu, K.; Zhang, J.; Ming, P.; et al. Antitumor efficiency of D-α-tocopheryl polyethylene glycol 1000 succinate-b-poly (ε- caprolactone-ran-lactide) nanoparticle-based delivery of docetaxel in mice bearing cervical cancer. *J. Biomed. Nanotechnol.* **2014**, *10* (8), 1509−1519.
(31) Fox, M. E.; Szoka, F. C.; Fréchet, J. M. J. Soluble polymer carriers for the treatment of cancer: the importance of molecular architecture. *Accounts Chem. Res.* **2009**, *42* (8), 1141−1151.
(32) Sahini, M. G. Polylactic acid (PLA)-based materials: a review on the synthesis and drug delivery applications. *Emergent Mater.* **2023**, *6* (5), 1461−1479.
(33) Begines, B.; Ortiz, T.; Pérez-Aranda, M.; Martínez, G.; Merinero, M.; Argüelles-Arias, F.; Alcudia, A. Polymeric nanoparticles for drug delivery: Recent developments and future prospects. *Nanomaterials* **2020**, *10* (7), 1403.
(34) Qi, L.; Xu, Z.; Jiang, X.; Hu, C.; Zou, X. Preparation and antibacterial activity of chitosan nanoparticles. *Carbohydr. Res.* **2004**, *339* (16), 2693−2700.
(35) Jeevitha, D.; Amarnath, K. Chitosan/PLA nanoparticles as a novel carrier for the delivery of anthraquinone: Synthesis, characterization and in vitro cytotoxicity evaluation. *Colloids Surf., B* **2013**, *101*, 126−134.
(36) Chang, C.; Zhang, L.; Miao, Y.; Fang, B.; Yang, Z. Anticancer and apoptotic- inducing effects of rutin-chitosan nanoconjugates in triple negative breast cancer cells. *J. Cluster Sci.* **2021**, *32* (2), 331−340.
(37) Chang, P. H.; Sekine, K.; Chao, H. M.; Hsu, S. H.; Chern, E. Chitosan promotes cancer progression and stem cell properties in association with Wnt signaling in colon and hepatocellular carcinoma cells. *Sci. Rep.* **2017**, *7* (1), 45751.
(38) Tomasina, J.; Lheureux, S.; Gauduchon, P.; Rault, S.; Malzert-Fréon, A. Nanocarriers for the targeted treatment of ovarian cancers. *Biomaterials* **2013**, *34* (4), 1073−1101.
(39) Zhu, H.; Chen, H.; Zeng, X.; Wang, Z.; Zhang, X.; Wu, Y.; Gao, Y.; Zhang, J.; Liu, K.; Liu, R.; et al. Co- delivery of chemotherapeutic drugs with vitamin E TPGS by porous PLGA nanoparticles for enhanced chemotherapy against multi-drug resistance. *Biomaterials* **2014**, *35* (7), 2391−2400.
(40) Jin, M.; Jin, G.; Kang, L.; Chen, L.; Gao, Z.; Huang, W. Smart polymeric nanoparticles with pH-responsive and PEG-detachable properties for co-delivering paclitaxel and survivin siRNA to enhance antitumor outcomes. *Int. J. Nanomed.* **2018**, *13*, 2405−2426.
(41) Alsehli, M. Polymeric nanocarriers as stimuli-responsive systems for targeted tumor (cancer) therapy: Recent advances in drug delivery. *Saudi Pharm. J.* **2020**, *28* (3), 255−265.
(42) Kulshrestha, R.; Singh, A.; Kumar, P.; Nair, D. S.; Batra, J.; Mishra, A. K.; Dinda, A. K. Nanoapproach targeting TGFβ1-Smad pathway and modulating lung microenvironment. *Process Biochem.* **2022**, *121*, 126−141.
(43) Dhanapal, J.; Ravindrran, M.; Baskar, S. Toxic effects of aflatoxin B1 on embryonic development of zebrafish (Danio rerio): Potential activity of piceatannol encapsulated chitosan/poly (lactic acid) nanoparticles. *Anti-Cancer Agents Med. Chem.* **2015**, *15* (2), 248−257.
(44) Rachmawati, H.; Yanda, Y. L.; Rahma, A.; Mase, N. Curcumin-loaded PLA nanoparticles: formulation and physical evaluation. *Sci. Pharm.* **2016**, *84* (1), 191−202.
(45) Guideline, I. H. T. Validation of analytical procedures: text and methodology Q2 (R1), 2005.
(46) Sharma, D.; Sharma, R. K.; Sharma, N.; Gabrani, R.; Sharma, S. K.; Ali, J.; Dang, S. Nose-to-brain delivery of PLGA-diazepam nanoparticles. *AAPS PharmSciTech* **2015**, *16*, 1108−1121.
(47) Suri, R.; Neupane, Y. R.; Mehra, N.; Nematullah, M.; Khan, F.; Alam, O.; Iqubal, A.; Jain, G. K.; Kohli, K. Sirolimus loaded chitosan functionalized poly (lactic-co-glycolic acid)(PLGA) nanoparticles for potential treatment of age-related macular degeneration. *Int. J. Biol. Macromol.* **2021**, *191*, 548−559.
(48) Dalmolin, L. F.; Khalil, N. M.; Mainardes, R. M. Delivery of vanillin by poly (lactic-acid) nanoparticles: development, characterization and in vitro evaluation of antioxidant activity. *Mater. Sci. Eng., C* **2016**, *62*, 1−8.
(49) Singla, P.; Mehta, R.; Berek, D.; Upadhyay, S. N. Microwave assisted synthesis of poly (lactic acid) and its characterization using size exclusion chromatography. *J. Macromol. Sci., Part A: Pure Appl.Chem.* **2012**, *49* (11), 963−970.
(50) Ge, H.; Hu, Y.; Yang, S.; Jiang, X.; Yang, C. Preparation, characterization, and drug release behaviors of drug-loaded ε-caprolactone/L-lactide copolymer nanoparticles. *J. Appl. Polym. Sci.* **2000**, *75* (7), 874−882.
(51) Ghaffarzadegan, R.; Khoee, S.; Rezazadeh, S. Fabrication, characterization and optimization of berberine-loaded PLA nanoparticles using coaxial electrospray for sustained drug release. *Daru, J. Pharm. Sci.* **2020**, *28*, 237−252.
(52) Lu, B.; Lv, X.; Le, Y. Chitosan-modified PLGA nanoparticles for control- released drug delivery. *Polymers* **2019**, *11* (2), 304.
(53) Mohammed, M.; Mansell, H.; Shoker, A.; Wasan, K. M.; Wasan, E. K. Development and in vitro characterization of chitosan-coated polymeric nanoparticles for oral delivery and sustained release of the immunosuppressant drug mycophenolate mofetil. *Drug Dev. Ind. Pharm.* **2019**, *45* (1), 76−87.
(54) Mittal, G.; Sahana, D. K.; Bhardwaj, V.; Ravi Kumar, M. Estradiol loaded PLGA nanoparticles for oral administration: effect of polymer molecular weight and copolymer composition on release behavior in vitro and in vivo. *J. Controlled Release* **2007**, *119* (1), 77−85.
(55) Lanao, R. P. F.; Jonker, A. M.; Wolke, J. G.; Jansen, J. A.; van Hest, J. C.; Leeuwenburgh, S. C. Physicochemical properties and applications of poly (lactic-co-glycolic acid) for use in bone regeneration. *Tissue Eng., Part B* **2013**, *19* (4), 380−390.
(56) Meimetis, L. G.; Giedt, R. J.; Mikula, H.; Carlson, J. C.; Kohler, R. H.; Pirovich, D. B.; Weissleder, R. Fluorescent vinblastine probes for live cell imaging. *Chem. Commun.* **2016**, *52* (64), 9953−9956.
(57) Liang, J.; Li, F.; Fang, Y.; Yang, W.; An, X.; Zhao, L.; Xin, Z.; Cao, L.; Hu, Q. Synthesis, characterization and cytotoxicity studies of chitosan-coated tea polyphenols nanoparticles. *Colloids Surf., B* **2011**, *82* (2), 297−301.
(58) Sahini, M. G. Polylactic acid (PLA)-based materials: a review on the synthesis and drug delivery applications. *Emergent Mater.* **2023**, *6* (5), 1461−1479.
(59) Salatin, S.; Maleki Dizaj, S.; Yari Khosroushahi, A. Effect of the surface modification, size, and shape on cellular uptake of nanoparticles. *Cell Biol. Int.* **2015**, *39* (8), 881−890.
(60) Walters, D. K.; Muff, R.; Langsam, B.; Born, W.; Fuchs, B. Cytotoxic effects of curcumin on osteosarcoma cell lines. *Invest. New Drugs* **2008**, *26*, 289−297.
(61) Hu, G.; Cai, Y.; Tu, Z.; Luo, J.; Qiao, X.; Chen, Q.; Zhang, W. Reducing the cytotoxicity while improving the anti-cancer activity of

https://doi.org/10.1021/acsomega.4c02983
ACS Omega 2025, 10, 170−180

silver nanoparticles through α- tocopherol succinate modification. *RSC Adv.* **2015**, *5* (100), 82050−82055.
(62) Casalini, T.; Rossi, F.; Castrovinci, A.; Perale, G. A perspective on polylactic acid-based polymers use for nanoparticles synthesis and applications. *Front. Bioeng. Biotechnol.* **2019**, *7*, 259.
(63) Bossio, C.; Abdel Aziz, I.; Tullii, G.; Zucchetti, E.; Debellis, D.; Zangoli, M.; Di Maria, F.; Lanzani, G.; Antognazza, M. R. Photocatalytic activity of polymer nanoparticles modulates intracellular calcium dynamics and reactive oxygen species in HEK-293 cells. *Front. Bioeng. Biotechnol.* **2018**, *6*, 114.
(64) Karanam, G.; Arumugam, M. K. Reactive oxygen species generation and mitochondrial dysfunction for the initiation of apoptotic cell death in human hepatocellular carcinoma HepG2 cells by a cyclic dipeptide Cyclo (-Pro-Tyr). *Mol. Biol. Rep.* **2020**, *47* (5), 3347−3359.
(65) Tian, S.; Saravanan, K.; Mothana, R. A.; Ramachandran, G.; Rajiv gandhi, G.; Manoharan, N. Anti-cancer activity of biosynthesized silver nanoparticles using Avicennia marina against A549 lung cancer cells through ROS/mitochondrial damages. *Saudi J. Biol. Sci.* **2020**, *27* (11), 3018−3024.
(66) Selvi, B. C. G.; Madhavan, J.; Santhanam, A. Cytotoxic effect of silver nanoparticles synthesized from Padina tetrastromatica on breast cancer cell line. *Adv. Nat. Sci. Nanosci. Nanotechnol.* **2016**, *7* (3), 035015.
(67) Naveen kumar, S.; Rajivgandhi, G.; Ramachandran, G.; Manoharan, N. A marine sponge Fascaplysinopsis sp. derived alkaloid fascaplysin inhibits the HepG2 hepatocellular carcinoma cell. *Frontiers in Laboratory Medicine* **2018**, *2* (2), 41−48.
(68) Abbas Momtazi-borojeni, A.; Behbahani, M.; Sadeghi-Aliabadi, H. Antiproliferative activity and apoptosis induction of crude extract and fractions of Avicennia marina. *Iran. J. Basic Med. Sci.* **2013**, *16* (11), 1203.
(69) Rajivgandhi, G.; Maruthupandy, M.; Quero, F.; Li, W. J. Graphene/nickel oxide nanocomposites against isolated ESBL producing bacteria and A549 cancer cells. *Mater. Sci. Eng., C* **2019**, *102*, 829−843.
(70) Du, C.; Guo, Y.; Cheng, Y.; Han, M.; Zhang, W.; Qian, H. Anticancer effects of torulene, isolated from Sporidiobolus pararoseus, on human prostate cancer LNCaP and PC-3 cells via a mitochondrial signal pathway and the down-regulation of AR expression. *RSC Adv.* **2017**, *7* (5), 2466−2474.

https://doi.org/10.1021/acsomega.4c02983
ACS Omega 2025, 10, 170−180